

## Spectroscopy of optical waveguiding layers

M. Kuneva\*, S. Tonchev

*Institute of Solid State Physics, Bulgarian Academy of Sciences, 72 Tzarigradsko Chaussee Blvd., 1784 Sofia, Bulgaria*

Received January 27, 2011; Revised April 12, 2011

The authors have shared a 20-years experience on spectroscopy of proton-exchanged waveguide layers in LiNbO<sub>3</sub> and LiTaO<sub>3</sub>. The methods include infrared absorption and reflection spectrometry, X-ray photoelectron spectroscopy (XPS), mode spectroscopy and micro & waveguide Raman spectroscopy. Mode spectra were used for the determination of phases in Li<sub>1-x</sub>H<sub>x</sub>NbO<sub>3</sub> and Li<sub>1-x</sub>H<sub>x</sub>TaO<sub>3</sub>. Vibration spectra allow some comparative and semi-quantitative estimations of the thickness of phase sub-layers to be made, as well as conclusions about the positions of diffused H-ions in the crystal lattice. XPS provides information about the composition at the waveguide surface.

The structural and compositional information delivered by each of these methods helps to create a more complete description of the structure and the properties of such layers. The interpretation of the results emphasizes on the phase content of waveguides obtained at different technological conditions. Such combined analysis can contribute to adjustment of fabrication conditions for obtaining of defined phase compositions needed for waveguide devices with improved stability and characteristics.

**Key words:** optical waveguides, spectroscopy, phase composition, proton exchange.

### INTRODUCTION

Being ferroelectric crystals with very attractive properties for integrated optics, LiNbO<sub>3</sub> (LN) and LiTaO<sub>3</sub> (LT) are widely used in this field. The electro-optical coefficients of both crystals are high:  $r_{33} = 30.5$  pm/V; their Curie temperature ( $T_c$ ) is 1090–1210 °C for LN and 540–700 °C for LT (depending on stoichiometry). LN has much stronger birefringence  $\Delta n_{o,e}$  and about three orders of magnitude lower threshold power (10 J/cm<sup>2</sup>) for optical damage in the visible region.

LN and LT belong to the trigonal crystal system. The unit cell of LN consists of planar sheets of oxygen ions, situated perpendicularly to the optical axis *c*. Oxygen ions from neighbouring sheets form octahedral interstices which are one-third filled by niobium ions and one-third vacant (V), ordered in the +*c* direction in the sequence: Li-Nb/Ta-V. The crystal structure of LT is similar. The large number of vacancies favors the penetration of other ions and their high mobility together with the high mobility of the crystal's own metal ions.

An optical waveguide is a light-guiding transparent layer of high refractive index surrounded by

regions of lower index. The confinement of the light and the spatial distribution of optical energy inside the guiding layer depend on the refractive index profile.

Proton exchange (PE) [1, 2] is a technology for waveguide fabrication in LiNbO<sub>3</sub> and LiTaO<sub>3</sub>. Going by the scheme:



it modifies the crystal surface by Li-H ion exchange forming a layer of several  $\mu\text{m}$  in depth with a large extraordinary index increase  $\Delta n_e$  ( $\Delta n_e \sim 0.12$  at 633 nm) and then with strong waveguiding and polarizing effect.

Development of devices in optoelectronics requires reproducible methods for obtaining of effective low-loss waveguides on or in the substrate material. The easy and fast obtaining of optical waveguides in the electro-optical crystal LiNbO<sub>3</sub> by proton exchange (PE) has motivated the attempts to adjust the technology for producing high-quality waveguides. The Li<sub>1-x</sub>H<sub>x</sub>MO<sub>3</sub> layer formed by Li-H ion exchange shows complex phase behavior (up to seven different crystallographic phases in LiNbO<sub>3</sub> –  $\alpha$ ,  $\kappa_1$ ,  $\kappa_2$ ,  $\beta_1$ ,  $\beta_2$ ,  $\beta_3$  and  $\beta_4$  and up to 6 ones in LiTaO<sub>3</sub> –  $\alpha$ ,  $\kappa$ ,  $\beta_1$ ,  $\beta_2$ ,  $\beta_3$  and  $\delta$ ) depending on the hydrogen concentration (value of *x*) [3, 4, 5]. The number and the type of different phase modifications in crystal

\* To whom all correspondence should be sent:  
E-mail: kuneva@issp.bas.bg

solid solutions  $\text{Li}_{1-x}\text{H}_x\text{NbO}_3$ , what actually is the proton-exchanged lithium niobate, are determined by the crystallographic orientation and the rate of substitution of  $\text{Li}^+$  by  $\text{H}^+$  ( $x$ ). Each phase originates as an individual sub-layer undergoing phase jumps with gradual change of  $x$ . In every single one of them  $\Delta n_e$  is a linear function of proton concentration. Within a phase transition, the value of  $\Delta n_e$  and/or of the deformations perpendicular to the surface change by leap. As in all cases of generation of new materials and devices, there is a requirement for materials characterization and analysis in all stages of development.

### MODE (M-LINE) SPECTROSCOPY

The obtaining of the mode spectrum is the main point of waveguide characterization. It implies measurement of the angles of different modes at the waveguide output and calculation of the effective refractive index  $n_{\text{eff}}$  for each propagating mode with resolution of  $\sim 10^{-4}$ .

Mode spectroscopy study was performed by using the two-prism coupling [6] of He-Ne laser ( $\lambda = 632.8$  nm) and the distribution of the refractive index  $\Delta n$  in the depth  $d$  of the waveguide layer (optical profile) was reconstructed from the set of effective mode indices by using the inverse Wentzel-Kramers-Brillouin method (IWKB) [7]. In the case of single-mode waveguides the mode spectra measurements were performed in two media (air and water) and the optical profile was reconstructed solving the two mode propagation equations for a step-like optical profile. The recognition of that function means to define the waveguide parameters – thickness, maximal value of refractive index and profile shape. The profile shape and the maximal value of the index change allow a preliminary

evaluation of the phase composition according to the phase model to be made for a definite substrate orientation (X, Y or Z).

Exemplary optical profiles are presented in Fig. 1. The preliminary evaluation of the phase composition could be made as follows:

The values of the extraordinary refractive index change  $\Delta n_e = 0.15$  for Z-1 and ZN-1 and its gradual change to 0.12 on the optical profiles of the waveguide lead to the suggestion that these waveguides should contain the  $\beta_4$ -phase which is characterized by a higher level of proton doping compared to monocrystalline  $\text{H}_x\text{Li}_{1-x}\text{NbO}_3$  ( $0.65 \leq x \leq 0.7$ ) [8]. The  $\beta_4$ -phase can exist only in Z-cut proton-exchanged lithium niobate and only together with the  $\beta_3$ - and  $\beta_1$ -phases of lower value of  $x$ :  $0.53 \leq x \leq 0.65$  for the  $\beta_3$ -phase and  $0.44 \leq x \leq 0.52$  for the  $\beta_1$ -phase. Thus, the waveguides Z-1 and ZN-1 consist of at least three  $\beta_i$ -phases:  $\beta_1$ ,  $\beta_3$  and  $\beta_4$ . The other Z-cut single-mode waveguide ZN-5 should be in  $\beta_1$ , ( $\beta_1+\beta_2$ ) or ( $\beta_1+\beta_3+\beta_4$ ) – phase since the value of  $\Delta n_e$  exceeds 0.12, indicating that  $\beta_i$ -phase or phases have been formed during the PE process [4].

The same considerations applied to the X- and Y-cut samples lead to the conclusion that X-3 contains a  $\beta_3$ -phase [4], which can be found only together with a  $\beta_1$ -phase. The  $\beta_4$ -phase could not be formed in X-cut  $\text{LiNbO}_3$  [9]. As in the case of ZN-5, the shape of the optical profile could not be followed since the waveguides are single-mode. The optical parameters of Y-2 correspond to the coexistence of  $\beta_1$  and  $\kappa_1/\kappa_2$  phases. Y-2 has a step-like optical profile with a maximal index change of  $\Delta n_e = 0.11$ . Thus, that waveguide should contain the  $\beta_1$ -phase – the only one which could be obtained by low-temperature direct proton exchange in Y-cut  $\text{LiNbO}_3$  [9].

### VIBRATION SPECTROSCOPY

It is widely accepted that the waveguide effect and the increased photorefractive resistance of PE-layers are due to OH group formation when protons interact with oxygen atoms of the crystal lattice [12]. OH groups exist not only in protonated, but also in as-grown crystals due to residual water, and their O-H bonds lie in the oxygen planes, perpendicular to the optical (Z) axis [13]. PE leads to the formation of OH groups which are oriented mainly in the oxygen (X-Y) planes of the  $\text{LiNbO}_3$  crystal (“in-plane” OH), as it is confirmed by IR spectroscopy [14]. In principle, OH-stretching vibrations investigations allow statements on the proton concentration in the crystal and on the positions of OH defects in the crystal lattice to be made.

A powerful method for studying structural phase transitions in solids is Raman spectroscopy. Raman

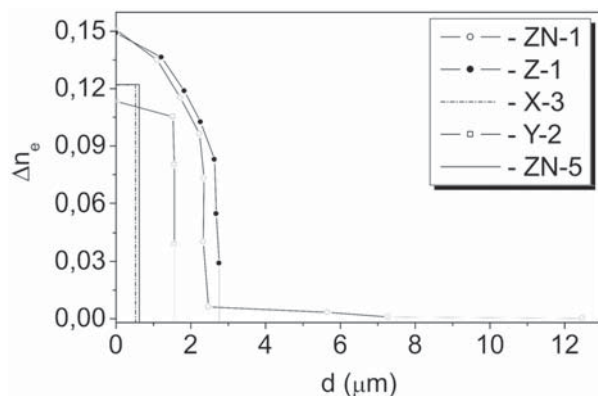


**Fig. 1.** Optical profiles of different PE waveguides in  $\text{LiNbO}_3$  [10, 11].

scattering is among the few experimental techniques that can answer questions concerning the phase state and phase transformations, deformations of the crystal lattice, and changes in the atomic configurations. With the development of integrated optics, it has become clear that the waveguide Raman technique is unique in studying the properties of thin waveguide layers [15].

Since the physical processes which determine the phonons active in Raman and infrared spectra also determine the electrooptical and the non-linear dielectric properties of materials, Raman and infrared (IR) spectra provide information for the characterization of the proton-exchanged layers.

#### *Infrared (absorption and reflection) spectroscopy*

IR absorption or transmission is very sensitive to H concentration in the crystal and hence offers a measure of the proton content before and after a partial or total doping. IR spectra of protonated and as-grown samples were recorded in the frequency range of 270–700  $\text{cm}^{-1}$  of OH-stretching modes with a Bruker LFS-113 V FTIR spectrometer and a Gaussian-Lorentzian decomposition procedure was performed. It was found that Gaussian deconvolution is better for highly protonated samples, but Lorentzian is better for virgin substrates. We have found also that the OH bands of protonated samples are better fitted by Gaussian profiles. Theoretically this different behavior is not surprising since the vibration spectrum of a disordered state – as the protonated crystal – is closely related to a Gaussian form.

After the decomposition, the frequencies and integrated intensities of the bands could be compared.

*IR spectra were used for:*

- Determining the crystal stoichiometry.
- Establishment of the OH bond orientation in the proton-exchanged layer (in or out of the oxygen planes) and therefore of the positions of the diffused hydrogen (in or out).
- Determining the thickness of the sub-layer which contains interstitial hydrogen (by stepwise polishing of the surface and recording the spectrum after each step).
- Following the changes in the phase composition and  $\text{H}^+$  presence during annealing procedures.
- Establishment of the phase composition of waveguides obtained by using different sources of protons (melts or vapors of different acidic compounds) or by modifying the PE technological conditions.

The structural studies of  $\text{LiNbO}_3$  single crystals [16] show that the oxygen anions are situated in the oxygen planes at three different distances from each other: 2.72, 2.88 and 3.36 Å, causing three compo-

nents in the IR absorption spectrum of the vibrations of OH groups in both  $\text{LiNbO}_3$  and  $\text{H:LiNbO}_3$ . The central peak is attributed to the O–O distance of 2.88 Å. It should be noted that the ratio of the band component intensities depends strongly on the crystal stoichiometry as far as the differences in crystal stoichiometry determine different surrounding.

While the modes of IR spectra of virgin and protonated  $\text{LiNbO}_3$  were well known from the literature, in the case of  $\text{LiTaO}_3$  such data were incomplete and this fact directed our efforts to the detailed investigation of the spectra before and after PE and to the determination of their dependence on stoichiometry.

The formula expressing the difference between the real crystal composition and the stoichiometric one can be written as:



The samples were selected to range through the whole interval of  $y = 0.012 \div 0.038$  ( $y = 0.033$  for congruent composition) which corresponds to Li mole fraction from 0.481 to 0.494.

Absorption IR spectra of three Z-cut samples  $\text{LiTaO}_3$  with different values of  $y$  are shown in Fig. 2, together with a schematic representation of the values of peak frequencies and intensities of the spectral components resulting from the Lorentzian decomposition procedure. The analysis of the results shows that three distinct closely spaced components at 3460, 3474 and 3484  $\text{cm}^{-1}$  exist and they can be assigned to O...O bonds of a length about 2.84–2.87 Å. When  $y$  increases (Li depletion), the components shift towards higher frequencies, the halfwidths of the components increase, the intensity of the higher frequency component (dominating in the case of stoichiometry composition) strongly decreases and the spectral structure becomes less pronounced. Optical measurements showed that Li depletion leads to lower values of  $\Delta n_e$ . This fact underlines the importance of crystal composition homogeneity for obtaining reproducible results and high performance of the waveguiding devices. For example, only a few percent changes in  $n_{\text{eff}}$  in the channels of a directional coupler can break down its action.

The dependence of IR spectra on stoichiometry could be used for approximated estimation of Li/Nb or Li/Ta ratio in virgin  $\text{LiNbO}_3$  and  $\text{LiTaO}_3$  or at least for quick identification of crystals of the same stoichiometry which is very important for reproducible technological results.

Infrared spectroscopy has proved its ability to characterize PE layers in  $\text{LiNbO}_3$  since the Li-H substitution dramatically increases the presence of OH groups in the exchanged layer. IR absorption in the range of OH stretching vibrations (2700–

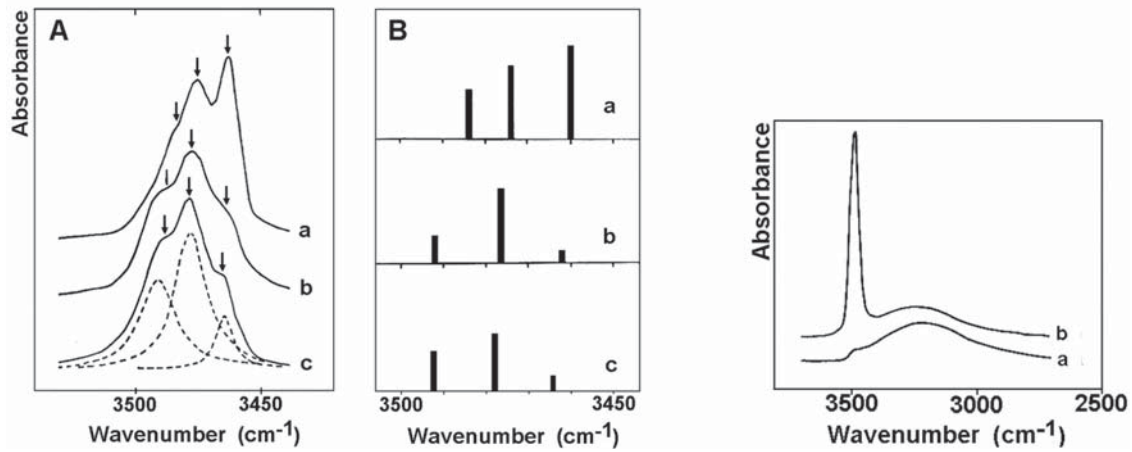


**Fig. 2.** OH absorption of virgin LT samples with different stoichiometry: a)  $y=0.012$ ; b)  $y=0.023$ ; c)  $y=0.038$ , and scheme of frequency positions and intensities of the components; polarized OH spectra of a X-cut LT sample: E||Z (a); E⊥Z (b)

3700  $\text{cm}^{-1}$ ) has been widely used for estimation of the phase composition [10, 17, 18, 19]. The spectra show several bands (at 3488  $\text{cm}^{-1}$ , 3500  $\text{cm}^{-1}$ , 3512  $\text{cm}^{-1}$ , 3250–3280  $\text{cm}^{-1}$ ) which could be attributed to different phases forming the PE layers [3]. It should also be noted that all the peaks except of a large shoulder at 3280  $\text{cm}^{-1}$  are polarized, showing that OH bonds lay in the oxygen planes of the crystal. The unpolarized band indicates the presence of hydrogen in interstitial positions out of the oxygen planes, which usually means a higher level of doping.

As it is known, a band centered at 3488  $\text{cm}^{-1}$  in the IR spectrum of proton-exchanged  $\text{LiNbO}_3$  is attributed to the  $\alpha$ -phase [4, 20]. All other bands could be assigned to the phases formed by PE: the broad

band centered at 3250–3280  $\text{cm}^{-1}$  – to the  $\beta_2$ ,  $\beta_3$  and  $\beta_4$  phases, the band at 3500  $\text{cm}^{-1}$  – to the  $\beta_i$  ( $i=1-3$ ),  $\kappa_1$  and  $\kappa_2$  produce peaks between 3488 and 3500  $\text{cm}^{-1}$  (intermediate values between  $\alpha$ -phase and  $\beta_1$ -phase) and are spectroscopically indistinguishable. For the strongly protonated samples, a fourth additional component emerges at about 3512  $\text{cm}^{-1}$  which could be attributed to the  $\beta_4$  only. Since the component due to the substrate  $\alpha$ -phase was extracted from the spectra after the deconvolution, only the components of the layers' spectra are present in the histograms (Fig. 3). Thereby the evolution of the bands assigned to different phases versus the variations in the technological parameters could be followed.

Thus, the histograms show not only the presence of definite phases, but also how the technological

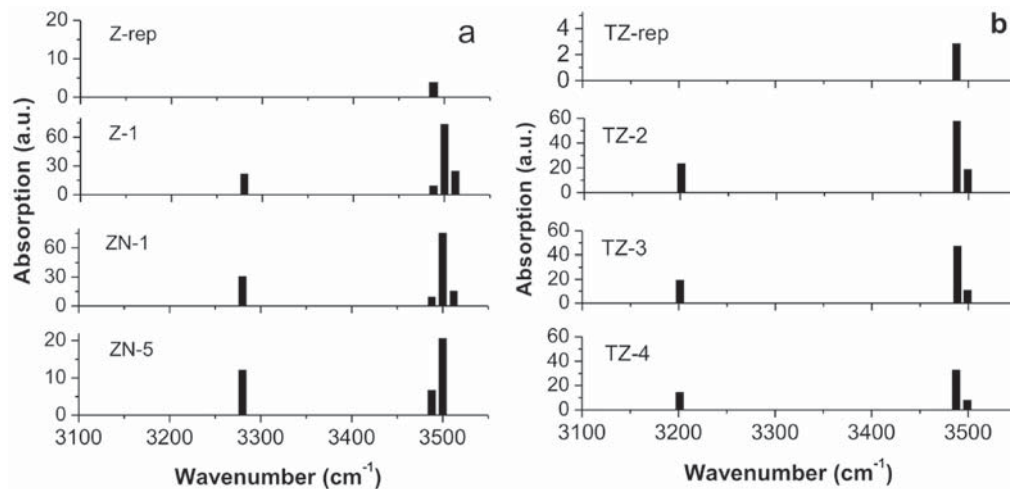


**Fig. 3.** Relative intensities of the IR-spectra components (after Gaussian decomposition) for PE layers in  $\text{LiNbO}_3$  (a) and  $\text{LiTaO}_3$  (b) obtained at different technological conditions [19]. Since the component due to the substrate  $\alpha$ -phase was extracted from the spectra after the deconvolution, only the components of the layers' spectra are present in the histograms

condition chosen reflects on the thickness of sublayers formed by these phases. It was established this way that the contribution of the  $\beta_4$ -phase is stronger in samples with higher  $\Delta n_o$ , i.e. higher level of proton doping. The contribution of  $\alpha/\kappa_1/\kappa_2$  is stronger in samples obtained at a condition including annealing or an annealing-like step. The contribution of  $\beta_1$  is stronger for samples obtained by direct proton exchange. We have found that the integrated intensity of OH spectra of PE waveguides does not change during annealing procedures, i.e. no loss but only redistribution of hydrogen ions takes place.

The polarization study (Fig. 2) showed that in PE layers the narrow bands lie in the plane perpendicular to the optical axis (Z) while the OH-bonds corresponding to the wide band are distributed both in and out of this plane. As in the case of H:LiNbO<sub>3</sub>, the main peak is connected with OH-bonds arranged in the oxygen planes (“in-plane” OH) and the shoulder – with OH bonds situated in the oxygen planes as well as out of them (hydrogen-bonded OH).

In order to shed some light on the proton distribution in our samples we have polished off the sample surface slightly and then, after each polishing step, we have measured the OH absorption. When a layer of  $0.1 \pm 0.2 \mu\text{m}$  thickness was removed, the shoulder in the spectra also disappeared, the central peak remaining almost unchanged.

On the basis of investigations on the polarized spectra, the following conclusions could be made:

1. The absorption band centered at  $3240 \text{ cm}^{-1}$  is due to a very thin surface layer while the  $3496 \text{ cm}^{-1}$  band is connected with the proton-exchanged layer extended much deeper in the crystal. The broad absorption band at  $3280 \text{ cm}^{-1}$  results from a very thin surface layer (about  $0.1\text{--}0.2 \mu\text{m}$ ); the strong band (peak at  $3496 \text{ cm}^{-1}$ ) is due to the protonated layer extending deeper.

2. The presence of the top film depends on the orientation of the sample, the X- and Y-cut plates being preferable.

3. The H concentration in the upper layer grows much more quickly in time, i.e. the  $\text{Li}^+ - \text{H}^+$  substitution there is more complete.

4. The layers have different crystal symmetries. The OH groups at the surface are randomly oriented and are connected with a variety of short hydrogen bonds. The OH groups in the depth of the basic layer are localized in the plane perpendicular to the Z-axis and are connected with moderate H bonds.

5. After annealing, the intensity of the unpolarized shoulder decreases since protons penetrating deeply in the crystal from out-plane bonds form new in-plane ones.

6. The evolution of IR spectra at different annealing stages indicates phase transitions from highly protonated phases to the original crystal structure ( $\alpha$ -phase).

7. Optical measurements and the study of IR absorption show that the H content in the waveguides is not influenced by the annealing procedures and the stoichiometry of the crystal, but only by the parameters of the exchange process.

8. It is difficult to observe any dependence on stoichiometry in the spectra of protonated LiNbO<sub>3</sub> or LiTaO<sub>3</sub> even if it really exists: the intensity of the band of PE crystals is about ten times higher than that of the virgin samples and slight variations in the spectra of untreated samples due to different stoichiometry cannot affect notably the final form of the spectra.

9. The intensities of the two bands depend on the PE process duration, demonstrating behavior usual for diffusion processes (Fig. 4). Proton concentration in the very surface layer increases much faster in time, i.e. there is a more complete replacement of Li ions by protons.

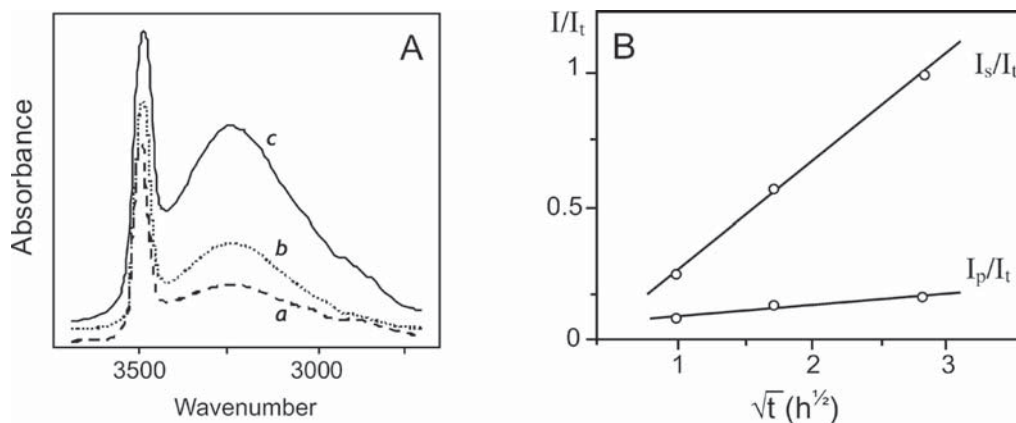


**Fig. 4.** A) OH absorption of X-cut LiTaO<sub>3</sub> (240 °C, pure benzoic acid) at PE duration of 1h (a), 3h (b) and 8h (c); B) Dependence of  $I_p/I_t$  and  $I_s/I_t$  on  $\sqrt{t}$  for X-cut LiTaO<sub>3</sub> (240 °C, pure benzoic acid);  $I_p$  and  $I_s$  are the integrated intensities of the bands at  $3496 \text{ cm}^{-1}$  and at  $3240 \text{ cm}^{-1}$  respectively,  $I_t = I_p + I_s$ ,  $t$  – exchange time.

10. The structures of the surface layer and that of the underlying protonated region are different. OH groups near the surface are chaotically oriented, indicating a great degree of disorder (amorphous state). The OH groups of the basic protonated layer are situated in the planes perpendicular to the optical axis. Lower frequency of the first kind of bonds implies higher mobility of their protons which could deteriorate the waveguide properties. So, the presence or the absence of a shoulder in IR spectra can serve as a criterion for the optical properties of waveguides fabricated by PE.

The PE waveguide stability in time can be followed by IR spectra and optical measurements. It was established that the behavior of integrated intensity in time is the same as this of  $\Delta n_c$  and IR spectra and can be used for studying the stability of waveguide parameters [21].

IR reflection spectra (Fig. 5) were recorded with the same spectrometer as for the absorption ones at angle of incidence  $70^\circ$  (measured from the normal to the surface). Since the penetration depth depends on the angle of incidence, at smaller angles (closer to the normal incidence) deeper penetration takes place and the spectra measurement is affected by the presence of the various phases forming the waveguiding layer. It was established [22] that at  $70^\circ$  the spectrum of the surface layer is separated from those of deeper situated layers in multiphase guides. This way, only the surface phase could contribute to the reflection spectra of multiphase waveguides. The IR reflection spectra contain new bands within the range  $890\text{--}1010\text{ cm}^{-1}$  and each phase has its own reflection spectrum [22, 23].

The IR reflection spectroscopy allows the surface phase of multiphase waveguides to be recognized. So, the information given by the analysis of the IR reflection spectra helps us to be much more specific when determining which phases build the waveguide layers investigated. According to [22], the presence

of  $\beta_i$ -phases significantly affects the spectra in the range of  $800\text{--}1000\text{ cm}^{-1}$  where new bands appear which are absent in the cases of virgin or  $\alpha$ -phase PE  $\text{LiNbO}_3$ . The characteristic changes are at  $975\text{ cm}^{-1}$  for  $\beta_1$ -phase, at  $980\text{ cm}^{-1}$  for  $\beta_2$  and  $\beta_3$ , and at  $970\text{ cm}^{-1}$  for  $\beta_4$  [22]. Thus, looking at the spectra of Fig. 5a, we could conclude that  $\beta_1$ -phase is present on the top of the sample ZN-5 while  $\beta_4$ -phase forms the top of the waveguide layers of samples ZN-1 and Z-1, which are really strongly protonated. Also, it is seen that the spectrum of ZN-5 is closest to the shape of the spectrum of virgin sample (Z-rep), which suggests that the contribution of the  $\alpha$ -phase is larger than in the case of the other two samples. This confirms the result of IR absorption spectra deconvolution, showing the same result (Fig. 3a). It could be seen that Z-1 and ZN-1 have almost the same spectra, confirming their equal phase content, as it could be seen also in Fig. 3a.

The main changes in the reflection spectra introduced by proton exchange in Z-cut  $\text{LiTaO}_3$  occur in the range of  $850\text{--}1050\text{ cm}^{-1}$  (Fig. 5b). They were compared to the spectra of X-cut PE  $\text{LiTaO}_3$  given in [23] and some correlations with lattice deformations and reflection minimums were made in order to assign the spectral changes to a definite phase. According to [23], the changes observed at  $899$ ,  $952$  and  $985\text{ cm}^{-1}$  in IR reflection spectra of all samples could be assigned to the  $\beta$ -phase, and the change at about  $1000\text{ cm}^{-1}$  to the  $\delta$ -phase, correspondingly. Since the second perturbation is much stronger, we should conclude that the surface phase of the waveguides investigated is  $\delta$ .

#### Micro-Raman and waveguide Raman spectroscopy

Proton exchange influences both vibration modes in Ra spectra  $A_1(\text{TO})$  and  $E(\text{LO})$  causing intensity reduction of some of the bulk lines, appearance

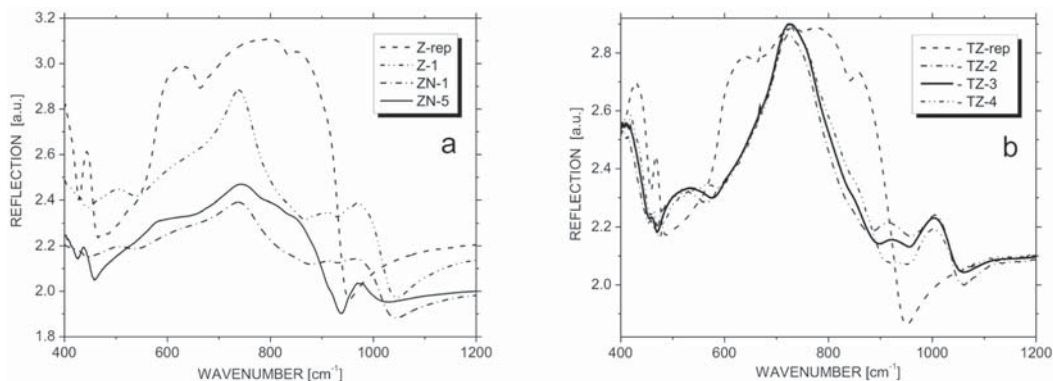


**Fig. 5.** Infrared reflection spectra for PE waveguides in  $\text{H:LiNbO}_3$  (a) and  $\text{H:LiTaO}_3$  (b) obtained under different technological conditions [19].

of new ones and appearance of lattice disorder-induced broad bands. A1(TO) type Ra spectra are more expressive.

In the Raman scattering geometries used, the phonon spectrum of pure LiNbO<sub>3</sub> consists of four A1(TO)-phonons (at 254, 275, 332 and 632 cm<sup>-1</sup>), polarized along the Z-axis, and seven E(TO)-phonons (at 152, 236, 263, 332, 370, 431 and 578 cm<sup>-1</sup>), polarized along the X- or Y-axis [24]. It could be seen in Fig. 6 that the main changes introduced by PE concern the intensity of the main spectral lines, the appearance of new ones and the spectra intensity attenuation compared to those of the surface. The strong attenuation occurs in samples with the maximal disorder degree [25]. The disorder in crystals causes violation of the selection rules which determine Raman scattering and can also activate new modes forbidden for the regular lattice. Moreover, as vibrations with  $k \neq 0$  of the material can take part into the light scattering, the Raman bands are broadened. On the other hand, the characteristic phonons of the pure crystal still exist in the spectrum, although they are considerably reduced in intensity.

According to [26], the most notable changes after PE are in band intensities in the 200–500 cm<sup>-1</sup> region and, most importantly, the appearance of a broad band in the 520–750 cm<sup>-1</sup> is observed, originating from a paraelectric-like phase, as well as the A1(TO)-peak at 690 cm<sup>-1</sup> and the bulk spectra intensity attenuation. [27]. The new band present in all spectra of our PE layers could be due to second-order Raman scattering [28] which is a combined Ra scattering from coexisting ferroelectric ( $\alpha$ ) and paraelectric ( $\beta$ ) LiNbO<sub>3</sub>. That way the Ra spectra give some evidence for the presence of  $\alpha$ -phase in the PE layer as the IR absorption spectra do (Fig. 3). The peak appearing

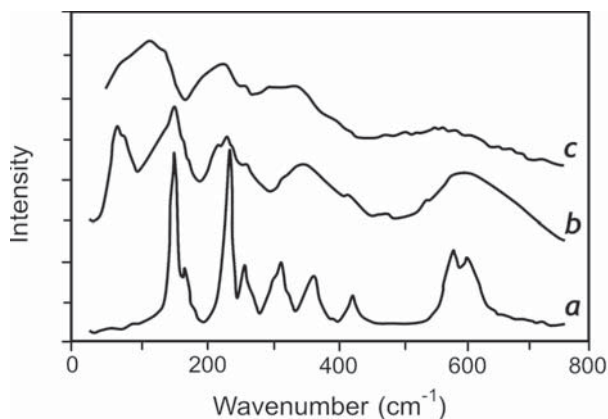


**Fig. 6.** Raman spectra of bulk LiNbO<sub>3</sub> in ferroelectric state at room temperature (a); H:LiNbO<sub>3</sub> waveguide (b) and bulk LiNbO<sub>3</sub> in paraelectric phase at 1130 °C (c); laser line at 647.1 nm, A1(TO) geometry

at 878 cm<sup>-1</sup> comes from E(LO) mode, excited due to the strained lattice, and confirms the high level of H<sup>+</sup>-doping. The set of narrow peaks in the Ra spectra also indicates high value of  $x$  and the presence of  $\beta_i$ -phases ( $i = 1-3$ ) [29].

The new peak which appears at 690 cm<sup>-1</sup> is attributed to highly protonated phases having almost paraelectric properties since it is characteristic for the paraelectric phase of LiNbO<sub>3</sub>. Its relative intensity allows some estimation of the phase contribution to the PE layers to be made. For our samples we can see this peak even in E(TO) spectra. As it is known, in strained crystal some coupling between E(TO) and A1(TO) modes is possible. Thus we could consider the presence of such large band as an evidence for the existence of phases having highest value of  $x$  as  $\beta_4$  for Z-cut samples,  $\beta_3$  for X-cut or  $\beta_1$  for Y-cut samples. For quantitative estimates it is important to obtain Raman scattering by guided modes in order to be sure that the optical power is confined completely into the waveguiding layer. If higher order modes are excited, part of the optical field penetrates more or less into the unprotonated substrate and this should be taken into account.

Raman scattering has also been used to determine the kinetics of phase transitions in proton-exchanged LN waveguide layers subjected to thermal treatment [30]. Results of fundamental importance have been obtained for intermediate phase states including the  $\beta_i$ - and ( $\alpha+\beta_i$ )-phases, as well as room-temperature equilibrium and quenched states in the high H<sup>+</sup> concentration phase. The presence and absence of some Raman lines at 127, 194 and 214 cm<sup>-1</sup> and the intensity dependence of a proton-induced phonon band at 69 cm<sup>-1</sup> have enabled the degree of Li-H substitution in PE layers to be determined, the results indicating that at least for z-cut H:LN waveguides, the phase diagram presented for proton-exchanged powders may also be applicable.

Besides waveguide Raman spectroscopy, micro-Raman spectra were also registered allowing some comparative and semi-quantitative estimations of the thickness of phase sub-layers to be made. The micro-Raman spectra were collected by triple Jobin Yvon T64000 spectrometer. Depth profiling of the proton-exchanged layer by Ra spectra was performed by moving the focused laser beam from the substrate to the surface of the layer at approximately 0.5 micrometer steps. An example is shown in Fig. 7.

An exemplary analysis of the spectra shown in Fig. 7 demonstrates that:

Since the spectrum of C1 contains the peaks characteristic for bulk LiNbO<sub>3</sub> in positions as well as in relative intensities, the  $\alpha$ -phase has a strong contribution to the layer composition. The intensity increase of the band centered at 632 cm<sup>-1</sup> could be

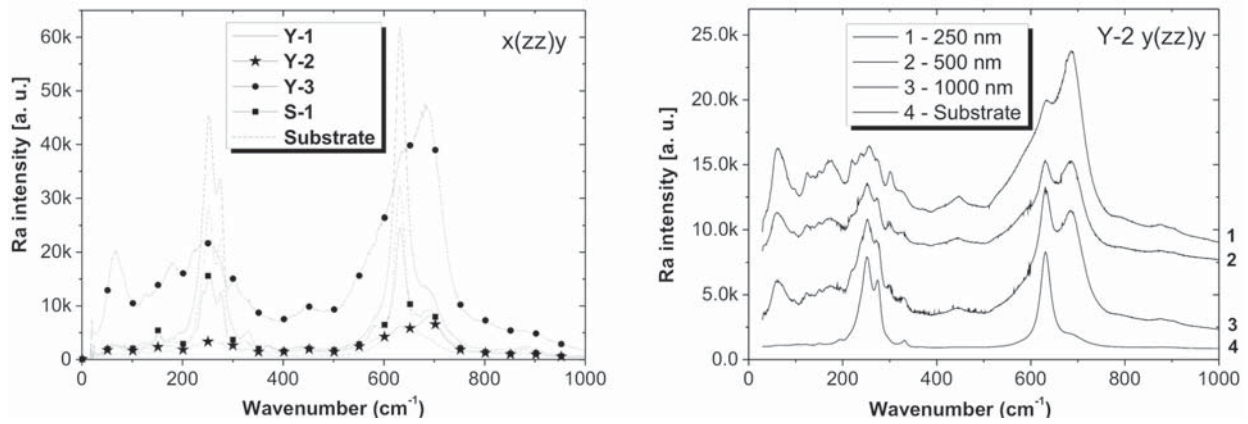


Fig. 7. Raman spectra of proton-exchanged Y-cut LiNbO<sub>3</sub> layers and micro-Raman depth profiling [21]

due to the presence of  $\alpha$  and  $\kappa_i$ -phases. The peak at 70 cm<sup>-1</sup> is present only in PE LN and usually is used as an indicator for Li-H exchange [27]. The new peak which appears at 690 cm<sup>-1</sup> is assigned to highly protonated phases having almost paraelectric properties ( $\beta_i$  phases,  $i = 1-3$ ). It suggests strong distortion of the niobium octahedra towards non-polar states. The broad band at 690 cm<sup>-1</sup> is characteristic for the paraelectric phase of LiNbO<sub>3</sub> [29]. Since the relative intensity of this band is not high, it could be concluded that the paraelectric layer is thin and is present at the top of the waveguiding layer, which is also confirmed by the optical profile shape. The peak appearing at 878 cm<sup>-1</sup> comes from E(LO) mode, excited due to the strained lattice, and also confirms the high level of H<sup>+</sup> doping. It could be assigned to the  $\beta_4$ -phase, since it is well defined only for samples C1 and S1 whose index change indicates the presence of that phase, leading to strong strains in the lattice.

The band centered at 690 cm<sup>-1</sup> is the highest and largest band in the spectra of C2. This fact, together with the disappearance of the bands at 245 cm<sup>-1</sup> and 275 cm<sup>-1</sup>, show that mainly phases having a high level of proton doping are present in the layer, i.e.  $\beta_i$  phases. In that case  $i = 1$ , since only the  $\beta_1$  phase could be obtained by direct PE [9].

The set of narrow peaks in the Ra spectrum of C3 and the new one which appears at 70 cm<sup>-1</sup> also indicate high value of  $x$  and the presence of  $\beta_i$  phases ( $i=1-3$ ) [29]. A broad band in the range of 520–780 cm<sup>-1</sup> is observed, originating from a paraelectric-like phase, as well as the A1(TO) peak at 690 cm<sup>-1</sup> and the bulk spectra intensity attenuation. Since C2 and C3 are obtained by direct proton exchange, the layer should consist of  $\beta_1$  phase but close to its higher concentration value of  $x = 0.6$ . That way the peak which appears at 690 cm<sup>-1</sup> is attributed to the  $\beta_1$  phase.

The spectrum of S1 confirms the presence of  $\beta_4$  on the top (peaks at 878 cm<sup>-1</sup> and 578 cm<sup>-1</sup> come from E(LO) modes, excited because of strong lattice perturbation introduced by PE). The spectra of C1 and S1 are quite similar, so we could conclude that S1 contains also some of the  $\beta_i$  phases,  $i = 1-3$ ,  $\kappa_i$  phases ( $i = 1-2$ ) and  $\alpha$  phase.

The most convenient way to determine the exchange ratio  $x/1-x$  in protonated layers is to decompose suitable parts of the Raman spectrum into ferroelectric and paraelectric components. In the case of the spectrum in Fig. 7 we have used the ferroelectric components 151 and 234 cm<sup>-1</sup> and their paraelectric counterparts – the broad bands at about 136 and 214 cm<sup>-1</sup> respectively. The ratio of their integrated intensities  $I(136)/I(151)=I(214)/I(234)$  should be equal to  $x/1-x$ .

The depth profiling of Y-2 (Fig.7) shows some intensity transfer between A1(TO) mode at 690 cm<sup>-1</sup> and E(TO) mode at 630 cm<sup>-1</sup>, which are excited in the same geometry because of the crystal lattice perturbation introduced by PE. The changes of E(TO) Ra spectra originate from the internal strains in the sample as a result of order-disorder distribution of protons, whereas the changes of A1(TO) Ra spectra are due to the displacement of the positive and negative ions [29]. Thus, in strongly protonated samples, the E(TO) intensities should be stronger and at the same time the A1(TO) intensities should be weaker. Since the intensity of the 690 cm<sup>-1</sup> band (A1) increases toward the substrate and that at 630 cm<sup>-1</sup> (E) decreases, we could conclude that the layer contains sub-layers, having different value of  $x$  (decreasing towards the substrate), i.e. presenting different phases in addition to  $\alpha$ - and  $\beta_1$ -phase, which was commented above. They should be  $\kappa_1/\kappa_2$  phases which are also indistinguishable spectroscopically.

## X-RAY PHOTOELECTRON SPECTROSCOPY (XPS)

X-ray photoelectron spectroscopy (XPS) is ideally suited to the determination of the surface chemistry and the way in which that chemistry changes in the surface and near-surface region. The technique provides quantitative elemental and chemical information with extremely high surface sensitivity and is ideal for comprehensively characterizing the elemental composition and chemical bonding states at surfaces and interfaces. It was shown how X-ray photoelectron spectroscopy (XPS) can be used for compositional analysis of the several uppermost atomic layers of the wafer apart from the waveguide/air interface in the case of proton-exchanged waveguides in lithium niobate [31, 32].

The XPS analysis of the samples was carried out with an ESCALAB Mk II (VG Scientific) electron spectrometer. The C1s, O1s, Nb3d and Li1s photoelectron peaks were recorded. A comparative analysis has been performed between virgin sample and layers obtained by PE in melts of pure benzoic acid and of benzoic acid buffered by 1% and 2% lithium benzoate. The goal was to clarify the dependence of crystal composition, Li1s, O1s and Nb3d spectra shape, binding energies (BE) and full width at half maximum (FWHM) in the near surface region (between 0 and 10 nm) on depth and on buffering of the benzoic acid melt with lithium benzoate. Using C1s as a reference at the surface, we determine the O1s position at 530.3 eV. In our investigation of the depth profile we use this binding energy as the reference since it is stable due to the fact that oxygen is a basic part of the LiNbO<sub>3</sub> lattice. The intensities were determined as the integrated peak

areas assuming that the background is linear. The element concentrations were calculated by the SSI (surface science instruments) approach according to which the transmission function of the analyzer is taken into account [33]. To avoid formation of a crater, the ion beam was defocused. A sputtering rate of 1 nm/min is established.

The most informative XPS spectra are those of LiO1s, and O1s which allow following of the binding energy change in the depth from the very surface to 500 nm of the exchanged layers versus the sputtering time (Fig. 8). The concentration of Li at the crystal surface could be estimated from XPS records and a correlation between  $x$  and  $\Delta n_c$  could be established when the optical profile is built up. It is seen that the Li content decreases and the Nb content increases with depth from the surface ( $d = 0$  nm,  $t = 0$  min.) to the first few atomic layers, lying close to the surface ( $d = 1-2$  nm), i.e. in a nearly two-dimensional region at the surface of the LiNbO<sub>3</sub> crystal. Enrichment of Nb with depth along with reduction of Li corresponds to reduction of the molar ratio of Li<sub>2</sub>O to Nb<sub>2</sub>O<sub>5</sub>. The composition remains nearly unchanged between 2 and 10 nm depth in the protonated layer.

The binding energy values are found to be almost equal when unbuffered benzoic acid melt is used instead of buffered melt (Fig. 9). It can be seen that the Li1s BE is lower at  $d = 1-10$  nm than at  $d = 0$  nm for unbuffered (0%) as well as for 1% and 2% buffered benzoic acid. For the virgin crystal, in contrast, BE increases at  $d = 1$  nm (compared to  $d = 0$  nm) and remains almost the same at 5 and 10 nm. The higher BE value obtained for 1% [34] than for 2% and 0% buffered melt at 1 nm depth is probably due to

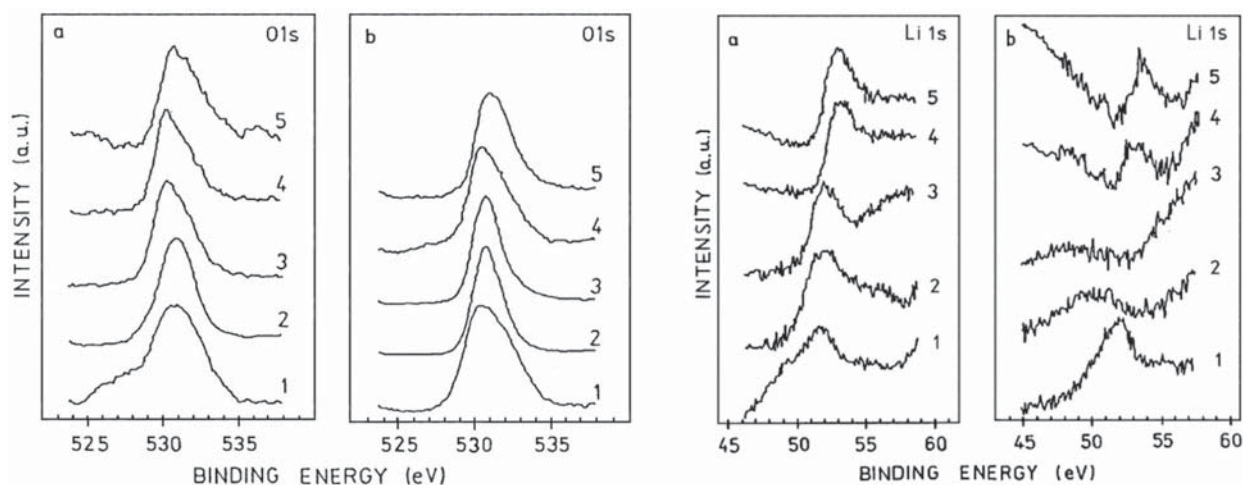


**Fig. 8.** The XPS spectra of a virgin (a) and PE (b) LiNbO<sub>3</sub> sample after sputtering to the following depths: 1) 0 nm (surface); 2) 10 nm; 3) 100 nm; 4) 200 nm; 5) 500 nm [34].

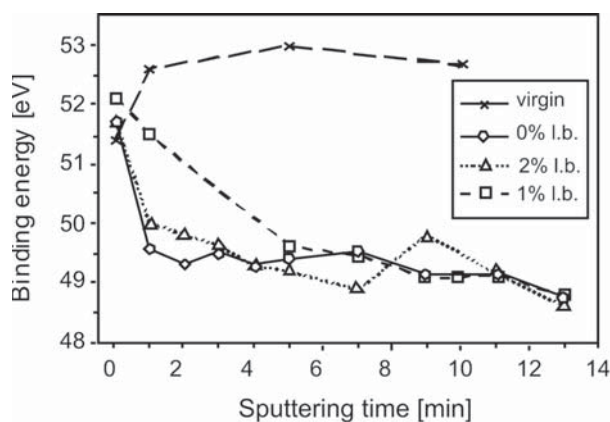


**Fig. 9.** Li 1s binding energy of LiNbO<sub>3</sub> versus depth (sputtering time) for unbuffered and for lithium benzoate (l.b.) buffered melts of benzoic acid, as well as for virgin LiNbO<sub>3</sub>

the fact that another LiNbO<sub>3</sub> crystal with different stoichiometry was investigated in [34]. The XPS spectra show that besides the main BE peaks lying between 49 and 53 eV for both treated and untreated samples, a weak peak appears at 54.8 eV for the sample protonated in buffered melt. This peak occurs only at  $d \leq 3$  nm and disappears at higher depths. Its BE value is close to the values obtained by Kaufherr et al. [35] where a non-destructive method was used. In comparison to the Li 1s, the BE depth dependence for O 1s is much less pronounced, especially when PE is performed in an unbuffered melt (Fig. 10). It may be explained with lower BE sensitivity to the changes in the surrounding due to the screening of the oxygen 1s electron from its 2s and 2p electrons. Regarding the change of the band's full width at half maximum (FWHM) with depth, it must be noted that the most evident decrease in comparison to  $d = 0$  nm appears at  $d = 1$  nm in the case of treatment with an unbuffered melt. In that case, some asymmetry of the peak at  $d = 1$  nm is also

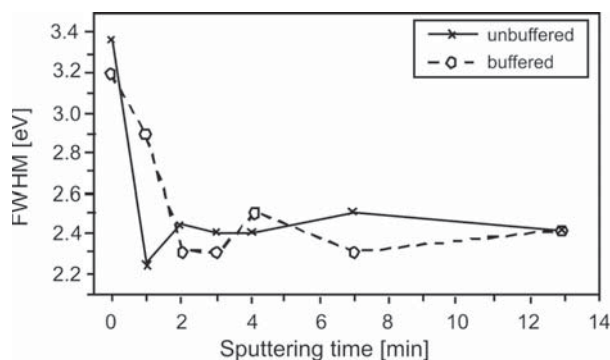
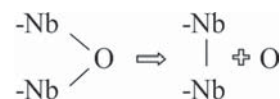


**Fig. 10.** Narrowing of the O 1s band of LiNbO<sub>3</sub> protonated in unbuffered benzoic acid melt

seen when normalized XPS spectra are compared. The FWHM changes described are probably due to superimposing of energetically close O 1s bands with different halfwidth and relative intensities. Such bands might correspond to weakly differing positions of the OH groups formed depending on depth and degree of protonation. Here it is worth mentioning that LiNbO<sub>3</sub> has two O 1s peaks with different relative intensities for the crystalline and amorphous state of the material as was already reported in Kaufherr et al. [35]. The experimental data for Nb XPS show that the peaks of the Nb<sup>5+</sup> doublet 3d<sub>3/2</sub> and 3d<sub>5/2</sub> at 207 and 210 eV respectively, are better resolved for  $d = 0$  nm than for the atomic layers in depth  $d = 1$  nm. This is also valid for the virgin LiNbO<sub>3</sub> [34], and could be related to a specific structure of the matrix surface layers which we supposed above to be responsible for the lower degree of protonation, i.e. the Li enrichment on the surface. Another explanation may be offered with the assumption that the surface structure is destroyed due to the sputtering and this is the reason for poorer peak resolution. Benzoic acid buffering has some influence on the BE values for the 207 and 210 eV peaks at depths of 1 nm which may be caused by differences in position and orientation of the OH groups toward the Nb atoms, depending on the degree of protonation. The intensity redistribution for the 207 and 210 eV peaks and the appearance of a new peak at 205 eV with increased sputtering time may be understood considering the results obtained in Courts et al. [36] on the reduction of Nb<sup>5+</sup> to Nb<sup>4+</sup> and Nb<sup>3+</sup>, when electron-beam heating of LiNbO<sub>3</sub> takes place. Before sputtering, the 205 eV peak is not observed because only Nb<sup>5+</sup> is present in our sample. The sputtering procedure of 1–2 min leads to the creation of some Nb<sup>4+</sup> and to superimposing of the low energy peak of the Nb<sup>4+</sup> doublet (i.e. Nb<sup>4+</sup> 3d<sub>3/2</sub>) at 205 eV. The higher energy peak Nb<sup>4+</sup> 3d<sub>3/2</sub> lies close to the 207 eV peak of Nb<sup>5+</sup> 3d<sub>3/2</sub> and is therefore not seen. Further accumulation of Nb<sup>4+</sup> on the crystal boundary takes place with increasing sputtering time and results at  $t > 4-5$  min in strong domination of the Nb<sup>4+</sup> 3d peaks at 205 and 207 eV. So, the Nb<sup>5+</sup> 3d<sub>3/2</sub> peak at 210 eV disappears and Nb<sup>5+</sup> 3d<sub>3/2</sub> at 207 eV is replaced by the Nb<sup>4+</sup> 3d<sub>3/2</sub> peak with almost the same BE. It has been established that the rate of intensity redistribution (increase for the 205 eV peak and decrease for the 210 eV peak) is higher in the case of the sample treatment with unbuffered benzoic acid melt. Probably NbO<sub>2</sub> or another Nb<sup>4+</sup> cluster compound with direct Nb-Nb bonding is formed on the surface due to the sputtering:



In summary, the study of proton exchanged (PE) LiNbO<sub>3</sub> performed using XPS after gradual removing of the surface atomic layers by Ar ion bombardment in depth (d) between 0 and 10 nm shows that:

– Noticeable differences regarding Li<sub>2</sub>O and Nb<sub>2</sub>O<sub>5</sub> molar ratio, Li1s binding energy values, O1s band width and Nb3d spectra shape are manifested at a depth of d = 1 nm as compared to d = 0 nm. Upon moving from d = 0 nm to d ≥ 1 nm, a decrease of Li content and Li1s BE lowering within 2 eV is revealed in the protonated sample, while for the virgin crystal Li1s BE increases with about 1 eV.

– In the depth range from 1 to 10 nm, only weak changes in Li and Nb content and in Li1s BE take place compared to d = 0-1 nm.

– These results allow us to conclude that a very thin layer on the LiNbO<sub>3</sub> crystal surface (about 3–4 atomic layers for X-cut samples) differs in structure and/or composition from the layers located deeper in the bulk. This layer has, as it is observed, a lower degree of H<sup>+</sup> for Li<sup>+</sup> substitution, i.e. a relative Li enrichment on the surface after the PE procedure.

– For PE being performed with unbuffered and buffered (containing 2% Li-benzoate) melts of benzoic acid, closely similar values of Li1s BE are obtained. This result shows that the Li content in the melt does not considerably affect the Li enrichment of the surface. Some influence of benzoic acid buffering is found for the O1s band width at d = 1 nm and for the BE of the Nb3d doublet which may be related to changes in position and orientation of the OH groups formed by the PE process.

## CONCLUSIONS

Combined analysis based on mode, IR absorption/reflection, Raman spectroscopy and XPS was performed which allows identification of phases, of the phase in-depth distribution, and of the relative contribution of each of them to the composition of the waveguide layer of multiphase proton-exchanged waveguides in lithium niobate and lithium tantalate.

The main results include:

– establishment of the effect of crystal stoichiometry on the parameters and vibration spectra of PE waveguides in LiNbO<sub>3</sub> and LiTaO<sub>3</sub>;

– improvement of the methods for investigation of phase composition of PE waveguides in lithium niobate and lithium tantalate by combination of several spectroscopic techniques (mode, Raman, infrared (absorption and reflection) spectroscopy, as well as XPS); application of this combined approach for characterization of the waveguide layers;

– following of the phase formation after proton exchange, phase evolution in time (short-term and

long-term) and phase transformations after thermal treatment (annealing);

– collection of information about the positions and concentration of the diffusant (H<sup>+</sup>).

The methods used could contribute to the improvement of the PE technology towards a strict control of the phase composition, i.e. of the waveguide characteristics and quality.

The results lead to the accumulation of new knowledge on material science regarding the properties of modified waveguiding layers on substrates of ferroelectric crystals.

## REFERENCES

1. J. L. Jackel, C. E. Rice, *Appl. Phys. Lett.*, **41**, 607 (1982).
2. W. B. Spillman, N. A. Sanford, R. A. Soref, *Opt. Lett.*, **8**, 497 (1983).
3. Yu. N. Korkishko, V. A. Fedorov, in: Proc. SPIE, 2700, 1996, 186.
4. Yu. N. Korkishko, V. A. Fedorov, *IEEE J. Select. Top. Quant. El.* 1 (1996).
5. K. El. Hadi, P. Baldi, S. Nouh, M. P. De Micheli, A. Leycuras, V. A. Fedorov, Yu. N. Korkishko, *Opt. Lett.*, **20**, 1698 (1995).
6. R. Ulrich, *J. Opt. Soc. Am.*, **60**, 1337 (1970).
7. J. M. White, P. E. Heidrich, *Appl. Opt.*, **15**, 151 (1976)
8. Yu. N. Korkishko, V. A. Fedorov, V. V. Nosikov, S. M. Kostritskii, M. P. De Micheli, in: Proc. SPIE, 2997, 1997, 188.
9. Yu. N. Korkishko, V. Fedorov, M. De Micheli, in: Proceedings of ECIO'97, April 2–4, Stockholm, 1997, 56.
10. M. K. Kuneva, S. Tonchev, M. Sendova-Vasileva, D. Dimova-Malinovska, P. Atanasov, *Sensors and Actuators A*, 99 (2002).
11. M. K. Kuneva, S. Tonchev, M. Pashtrapanska, I. Nedkov, *Materials Science in Semiconductor Processing*, **3**, 581 (2001).
12. C. E. Rice, *J. Sol. St. Chem.*, **64**, 188 (1986).
13. L. Kovacs, V. Szalary, R. Capriletti, *Solid State Communications*, **52**, 1029 (1984).
14. K. K. Wong, A. C. G. Nutt, D. F. Clark, P. J. R. Layborn, R. M. De La Rue, in: IEE Proc. Part I 133, 1986, 113.
15. I. T. Savatinova, S. Tonchev, E. Popov, E. Liarokapis, C. Raptis, *J. Phys. D: Appl. Phys.*, **25**, 106 (1992.)
16. J. R. Herrington, B. Dischker, A. Rauber, J. Schneider, *Solid State Communications*, **12**, 351 (1973).
17. M. K. Kuneva, S. Tonchev, E. Thatsi, D. Lampakis, *JOAM*, **7**, 549 (2005).
18. M. K. Kuneva, S. Tonchev, P. Dimitrova, *J. Mater. Sci.: Materials in Electronics*, **14**, 859 (2003).
19. M. K. Kuneva, S. Tonchev, P. Atanasov, *Mat. Sci. Eng. B*, **118**, 301 (2005).
20. J. Rams, M. Cabrera, *J. Opt. Soc. Am. B*, **16**, 401 (1999).

21. M. Kuneva, S. Tonchev, B. Bozhkov, *JOAM*, **11**, 1529 (2009).
22. Yu. N. Korkishko, V. A. Fedorov, S. M. Kostritskii, *J. Appl. Phys.*, **84**, 2411 (1998).
23. S. M. Kostritskii, Yu. N. Korkishko, V.A. Fedorov, D. B. Maring, R. F. Tavlykaev, R. V. Ramaswamy, *J. Appl. Phys.*, **91**, 930 (2002).
24. X. Yang, G. Lan, B. Li, H. Wang, *phys. stat. sol. (b)*, **141**, 287 (1987).
25. X. Wu, M.-S. Zhang, D. Feng, *Appl. Phys. Lett.*, **65**, 2916 (1994).
26. G. R. Paz-Pujalt, D. D. Tuschel, *Appl. Phys. Lett.*, **62**, 3411 (1993).
27. Yu. Voron'ko, A. Kudryavtsev, V. Osiko, A. Sobo, E. Sorokin, *Sov. Phys. Solid State*, **29**, 771 (1987).
28. R. Claus, G. Borstel, E. Wiesendanger, L. Stefan, *Z. Naturf.*, **27a**, 1187 (1972).
29. X.-L. Wu, M.-S. Zhang, D. Feng, *phys. stat. sol. (a)*, **153**, 233 (1996).
30. I. Savatinova, S. Tonchev, M. Kuneva, E. Liarokapis, *Appl. Phys. A*, **58**, 481 (1994).
31. M. K. Kuneva, V. Krastev, *J. Mater. Sci.: Materials in Electronic*, **11**, 629 (2000).
32. M. K. Kuneva, V. Krastev, *Cryst. Res. & Technol.*, **30**, K61 (1995).
33. L. T. Weng, *Surf. Interface Anal.*, **20**, 179 (1993).
34. M. Kuneva, V. Krastev, *Appl. Phys. A*, **63**, 391 (1996).
35. N. Kaufherr, D. J. Eichorst, D. A. Payne, *J. Vac. Sci. Technol. A*, **14**, 299 (1996).
36. R. Courths, P. Steiner, H. Höchst, S. Hüfner, *Appl. Phys.*, **21**, 345 (1980).

## СПЕКТРОСКОПИЯ НА СЛОЕВЕ ОПТИЧНИ ВЪЛНОВОДИ

М. Кънева, С. Тончев

Институт по физика на твърдото тяло „Акад. Г. Наджаков“,  
бул. Цариградско шосе 72, 1784 София

Постъпила на 27 януари, 2011 г.; приета на 12 април, 2011 г.

(Резюме)

Авторите споделят своя 20-годишен опит за спектроскопията на протонно-обменени вълноводни от  $\text{LiNbO}_3$  и  $\text{LiTaO}_3$ . Методите включват инфрачервена спектроскопия на абсорбция и отражение, микро-Раман и Раман спектроскопия и рентгенова фотоелектронна спектроскопия (XPS).

Информацията (структурна, фазова и химичен състав) получена от всеки от тези методи помага за създаване на по-пълно описание на структурата и свойствата на тези слоеве. Интерпретацията на резултатите набляга на фазите и химичния състав на вълноводите, получена при различни технологични условия. Такъв „комбиниран“ анализ допринася за регулиране на производството условията за получаване на определени състави и фази, технологично необходими за вълноводни устройства с подобрена стабилност и характеристики.